

1
2
3
4
5
6
7
8
9
10
11
12
13
14
15
16
17
18

**Characteristics of Monsoon Inversions over Arabian Sea observed by Satellite Sounder and
Reanalysis data sets**

Sanjeev Dwivedi¹, M. S. Narayanan¹, M. Venkat Ratnam^{2*} and D. Narayana Rao¹

¹Department of Physics, SRM University, Kattankulathur, Chennai - 603 203, India.

²National Atmospheric Research Laboratory (NARL), Gadanki, Tirupati- 517 502, India.

* vratnam@narl.gov.in ; Phone: +91-8585-272123; Fax: +91-8585-272018

19 **Abstract**

20 Monsoon inversion (MIs) over Arabian Sea (AS) is one of the important characteristics
21 associated with the monsoon activity over Indian region during summer monsoon season. In the
22 present study, we have used five years (2009 - 2013) data of temperature and water vapor
23 measurements obtained from satellite sounder instrument, Infrared Atmospheric Sounding
24 Interferometer (IASI) onboard MetOp satellite, besides ERA - Interim data, to study their
25 characteristics. The lower atmospheric data over the AS have been examined first to identify the
26 areas where monsoon inversions are predominant and occur with higher strength. Based on this
27 information, a detailed study has been made to investigate their characteristics separately in eastern
28 AS (EAS) and western AS (WAS) to examine their contrasting features. The initiation and
29 dissipation times of MI, their percentage occurrence, strength etc., has been examined using the huge
30 data base. The relation with monsoon activity (rainfall) over Indian region during normal and poor
31 monsoon years is also studied. WAS ΔT values are ~ 2 K less than those over the EAS, ΔT being
32 temperature difference between 950 and 850 hPa. A much larger contrast between WAS and EAS in
33 ΔT is noticed in ERA-Interim dataset vis a vis those observed by satellites. The possibility of
34 detecting MI from another parameter, refractivity N, obtained directly from another satellite
35 constellation of GPS RO (COSMIC), has also been examined. MI detected from IASI and
36 Atmospheric InfraRed Sounder (AIRS) sounder onboard NOAA satellite have been compared to see
37 how far the two data sets can be combined to study the MI characteristics. We suggest MI could also
38 be included as one of the semi-permanent features of southwest monsoon along with the presently
39 accepted six parameters.

40

41 *Keywords:* Monsoon inversion, Arabian sea, lower atmospheric temperature, satellite sounders,
42 IASI, ERA

43

44

45 **1. Introduction**

46 The Monsoon Inversion (MI) is one of the criteria providing a stability condition over the
47 western Arabian Sea (AS), extending sometimes through to the west coast of India. The MI controls
48 the mid tropospheric moisture content during the different phases of the monsoon. This shallow layer
49 of low level inversion (below ~ 800 hPa) will act as a barrier in uplifting of the moisture, and could
50 act like a wave – guide for transport of water vapour to the mainland. The fluctuation of the rainfall
51 over the west coast of India is more closely related to changes in monsoon circulation over the AS
52 (Das, 2002). The AS is located at the north head of the Indian Ocean. During the monsoon season,
53 Indian rainfall is dependent on the physical processes occurring over AS like SST, Somali Low
54 Level Jet and the advection of hot air from the Arabian desert. These have profound effect on
55 strength of MI. Thus, MI has been known to be intimately associated with the activity of the Indian
56 southwest monsoon and has a close link with active and break spells (Narayanan and Rao, 2004).

57 MIs were first detected in 1964 during International Indian Ocean Expedition (IIOE) from
58 ship radiosonde data by Colon (1964) and Ramage (1966). Subsequently from satellite derived
59 temperature and humidity data, this feature was detected by Narayanan and Rao (1981). They
60 detected MI despite the coarse vertical resolution (~ 2 km) of the TIROS – N satellite temperature
61 sounding instruments (Thomas,1980) of 1970 – 80s compared to the vertical extent (about 1 to 1.5
62 km) of the phenomena itself. They used a simple differencing technique by finding the difference,
63 ΔT , of sea skin temperature and 1000 to 850 hPa mean layer temperature (MLT) from the satellite
64 sounding data. By adopting this differencing procedure, they assumed that most of the systematic
65 errors/limitations of retrieval methods and vertical resolution of satellite soundings may be getting
66 significantly minimized. Furthermore, the spatial and temporal nature of MIs is quite large compared
67 to normal boundary layer inversions observed over land and other oceans.

68 Using data of about 150 ship radiosonde and aircraft dropsonde profiles and concurrent
69 TIROS – N satellite sounder data of MONsoon EXperiment (MONEX) conducted in 1979, they

70 showed that regions with $\Delta T \leq 2$ K in satellite derived atmospheric temperatures are associated with
71 AS MI. Study of these MIs over the western AS was one of the three major objectives of MONEX /
72 FGGE -1979 (WMO, 1976). These are seen to be much stronger (temperature departures from
73 normal profiles in some cases being as high as ~ 6 K in the lower 1 - 2 km height region) in contrast
74 to the inversions observed over land or associated with trade wind inversions ($\sim 1 - 2$ K).

75 MIs are characterized by both a vertical temperature increase in the altitude region from 0.5
76 km (in some cases even from surface) to ~ 2 km and with a sharp fall in relative humidity (RH)
77 above this altitude region. Some of the observed features of MIs reported from the limited
78 observations to date (Colon, 1964; Ramage, 1966; Narayanan and Rao, 1981; 1989) are: (i) strength
79 decreases and base increases from west to east AS, (ii) oscillation of its lateral boundary from west to
80 east with the activity of monsoon and (iii) associated oscillation of mid tropospheric water vapor
81 content from east to west, i.e. opposite to the boundary of temperature inversion. The two primary
82 causes proposed (Colon, 1964) for formation/maintenance of monsoon inversion are: (a) hot air
83 advection from Arabia (~ 700 hPa) riding over cool maritime air (at levels below ~ 800 hPa) from
84 south Indian Ocean and (b) subsidence over western AS associated with monsoon convection over
85 the Indian main land. This large scale subsidence had played a major role in the maintenance of MI
86 during the prolonged weak monsoon of 2002 (Narayanan et al., 2004).

87 However, not much attention was paid to the study of MI due to paucity of freely available
88 data over this region. The spatial density of TIROS – N satellite data available to the global research
89 community in 1979 was just a single temperature – humidity profile a day in a latitude – longitude
90 grid box of $2.5^\circ \times 2.5^\circ$ (Kidder et al., 1995). Narayanan and Rao (1981) had to adopt temporally a
91 pentad and spatially a $5^\circ \times 5^\circ$ average to detect statistically significant results from the meager data
92 available then. Since 2008, the number of temperature and humidity profiles from polar orbiting
93 satellites is nearly two orders of magnitude higher (about one vertical profile every 50×50 km, twice
94 each day and from two satellites) besides with a much better vertical and spectral resolution. Thus, it

95 has become possible now to study MI phenomena in greater detail. However, no in-situ data after the
96 1979 experiment are available in this region.

97 In the present study, we have used the high resolution and better accuracy temperature and
98 humidity profiles data obtained from Infrared Atmospheric Sounding Interferometer (IASI) onboard
99 MetOp satellite. These data have higher vertical resolution, i.e., ~ 400 m below 700 hPa, which is
100 much better than those of TIROS – N of MONEX 1979 period. Further, ERA-Interim data have been
101 used to compare the MI features seen in them with those from the satellite data. For explaining the
102 relative contribution of subsidence and convection on MI, wind observations from ERA-interim
103 reanalysis data have been used. The temperature - humidity profile data are also available from
104 NOAA – Atmospheric InfraRed Sounder (AIRS) instrument since 2002, all of which have also been
105 analysed in the same way as the IASI data. However, we have not presented those results here,
106 because of some inconsistencies (i.e. sometimes ERA – interim data shows MI but AIRS has
107 different features like no presence of MI, profile to profile match between AIRS and ERA-interim
108 datasets are not seen i.e. inversion type changes or level of inversion changes) observed between the
109 IASI and AIRS data in studying the MI features. Thus, we have confined the present study to data
110 only from one instrument, viz., IASI, which had been reported to be performing better (Smith et al.,
111 2015). This is expected to also ensure that the results of temporal and spatial gradients of ΔT
112 presented here (featuring MI) will be mutually consistent – even if the absolute values of
113 temperature/humidity may be having some errors. We have, however, included one section
114 comparing the results of these two instruments for studying the MI features. We have also shown to a
115 limited extent the potential of the GPS RO measured ‘refractivity’ profiles in delineating inversion
116 regions. For this we have also used the MONEX in-situ temperature – humidity profiles of 1979.

117 **2. Data**

118 As mentioned earlier, data from a variety of instruments have been used in this study – IASI
119 satellite instrument, ERA-Interim reanalysis data and, in-situ dropsondes/ radiosondes data obtained

120 during MONEX – 1979. Limited AIRS sounder data and GPS RO data have also been presented for
121 comparison purposes. A short description of each of these data is given in the following sub-sections
122 and is also summarized in Table 1.

123 **2.1. IASI observations**

124 IASI is a thermal infrared nadir-looking Fourier transform spectrometer which measures the
125 Earth's surface and the atmospheric radiation over a spectral range of 645–2760 cm^{-1} with a 0.5 cm^{-1}
126 spectral resolution. The IASI field of view is a matrix of $2^\circ \times 2^\circ$ circular pixels, each with a diameter
127 footprint of 12 km at nadir. It measures on an average at each location on the Earth's surface twice a
128 day (at 09:30 and 21:30 hr local time), every 50 km at nadir, with an excellent horizontal coverage
129 due to its polar orbit and its capability to scan across track over a swath width of 2200 km. The IASI
130 instrument (Clerbaux et al., 2007; 2009) measures temperature profiles in the troposphere and lower
131 stratosphere with a high accuracy ($\sim 1\text{K}$ root mean square) at a vertical resolution of 1 km in the
132 lower troposphere), as well as humidity profiles in the troposphere (10–15% accuracy with a 1–2 km
133 vertical resolution) primarily for numerical weather prediction (Schlüssel et al., 2005). More details
134 about retrieval and validation are presented in Kwon et al. (2012). The support products, which we
135 have used, are available at 100 pressure levels at 50 x 50 km horizontal grid spacing, but we restrict
136 the data from surface to 600 hPa for our analysis..

137 **2.2. Dropsonde / Radiosonde measurements MONEX (1979)**

138 For the in-situ ground truth comparisons over AS between the longitudes 55° - 75°E we also
139 make use of the aircraft dropsondes and ship radiosonde observations obtained during MONEX
140 1979. MONEX was conducted during May - July 1979 and there were 416 radiosondes and 412
141 dropsondes measurements over AS. It may be noted that after the MONEX campaign in 1979, no
142 campaign has been organized to get in-situ data over western or central AS. During the Indian
143 ARMEX programme (2002), however, some in-situ data were available but only in the far eastern
144 AS (east of 70°) near the coast of India. Table 2 summarizes the comparison of in-situ observations

145 with satellite data of 1979 by Narayanan and Rao (1981). This information on ΔT criterion has been
146 used as the reference in the present study. In this regard it is worth to quote recent study by Dwivedi
147 et al. (2016) who has reported observations of temperature inversions during July - August over
148 Muscat and Salah (east Arabia coast) from concurrent radiosonde and IASI data.

149 **2.3. ERA-Interim data**

150 The European Centre for Medium Range Weather Forecasts (ECMWF)-Interim is one of
151 most advanced in operational use for diagnosing the global atmosphere with an accuracy that is less
152 than what is theoretically possible (Simmons and Hollingsworth, 2002; Simmons et al., 2007). The
153 selected variables are specific humidity along with the temperature on different pressure levels. The
154 atmospheric data are available at $0.125^\circ \times 0.125^\circ$ latitude and longitude grids on 37 pressure levels
155 from 1000 to 1 hPa; however, we have used for the present study, data of 14 pressure levels from
156 1000 to 600 hPa for the period of 2009 to 2013. . Vertical as well as horizontal strength of MI have
157 been examined from these data sets and compared with satellite observations.

158 **2.4. AIRS observations**

159 AIRS onboard the Earth Observing System (EOS) - Aqua satellite of NASA was launched in
160 2002. This is also a polar orbiting satellite which crosses the equatorial latitudes at 13:30 hr LT and
161 01:30 hr LT for the ascending and descending passes, respectively. The orbit period is 98.99 min,
162 and the orbit is sun synchronous with consecutive orbits separated by 2760 km at the equator. AIRS
163 has a field of view of 1.1° and provides a nominal spatial resolution of 13.5 km for IR channels and
164 approximately 2.3 km for visible/near-IR channels. AIRS data together with data from the Advanced
165 Microwave Sounder Unit (AMSU) (Lambrigtsen, 2003) are used. We make use of AIRS support
166 data which have higher vertical resolution with 100 levels between 1100 and 0.016 hPa. In this
167 study, we use the data from surface to 600 hPa which have vertical resolution of 30-20 hPa. These
168 data are available since 2003. We use data from 2009 - 2013 to compare with other data sets.

169

170 **2.5.COSMIC GPS RO**

171 GPS RO technique is also a remote sounding satellite technique, and it uses the radio signals
172 received onboard a low Earth orbiting satellite from atmospheric limb sounding. The GPS RO
173 measurements have a vertical resolution ranging from 400 m to 1.4 km, which is much better than
174 that of any other satellite data (Kursinski et al., 1997). COSMIC has vertical resolution of ~ 100 m in
175 the lower troposphere for temperature. The COSMIC GPS RO was successfully launched in mid-
176 April 2006 (Anthes et al., 2008). Since 17 July 2006, COSMIC GPS RO provides accurate and high
177 vertical resolution profiles of atmospheric parameters that are almost uniformly distributed over the
178 globe. COSMIC provides a direct estimate of refractivity (from measurement of bending angle by
179 GPS technique) at very high vertical resolution, but have poor repetivity.

180

181 **3. Methodology and analysis procedure**

182 As mentioned earlier, MI was first observed by Colon (1964) and Ramage (1966) over the
183 AS from ship upsonde profiles. They reported that MI lies between 900 and 800 hPa with strong
184 intensity over western AS (WAS) and weakens as its base rises and moves to eastern AS (EAS).
185 Following this study, Narayanan and Rao (1981) have shown MIs presence using the temperature
186 difference (ΔT) between the TIROS-N derived sea skin temperature and atmospheric layer mean
187 temperature (between 1000 hPa and 850 hPa).

188 Note that lapse rate (dT / dz) of atmosphere at the tropospheric altitudes is a negative
189 quantity. However, in this study (and also in Narayanan and Rao, 1981), we have considered ΔT as
190 the temperature difference between a lower level (higher temperature) and a higher level (lower
191 temperature), so is a positive quantity between ~ + 6 and + 7 K. For inversion regions, it is negative
192 or a small positive quantity (i.e. less than + 2 K).

193 After considering several limitations in the satellite data of that time, Narayanan and Rao
194 (1981) finally considered MI when the difference ΔT , between surface and layer mean temperature

195 (of 1000 to 850 hPa), is 2 K or less, which otherwise was greater than 3 K. Since then, several
196 improvements in the satellite instruments, retrieval techniques and data products have come up in
197 these three decades.

198 Extensive AS MI features were observed from in-situ measurements during FGGE-MONEX
199 1979 experiment. Fig. 1a shows a typical example of MI observed in T and RH (Relative Humidity)
200 data obtained on 27 June 1979 at 0656 GMT at 20°N, 62°E from radiosonde. In this example MI
201 starts from surface and temperature departure is as high as ~ 10 K from a normal lapse rate profile at
202 900 hPa. The vertical extent of inversion varies from 0.5 km to even more than 1 km. It is to be
203 noted that AS MI are much stronger and long lasting i.e. less diurnal variation than normal boundary
204 layer and persist for many days compared to those over land regions.

205 A detailed analysis is made in this study by considering several thousands of profiles
206 obtained from different satellite observations now available over AS for in depth study of MI. Since
207 the MIs occur at low levels, first we tried with the earlier adopted criteria of Narayanan and Rao
208 (1981) i.e., by taking difference between sea surface (skin) temperature and 925 hPa level (mean
209 pressure level of 1000 - 850 hPa MLT of TIROS-N data of the 1980 time frame) temperature and
210 found those to be noisy for detecting MI. To avoid the surface emissivity effects in the retrieval at /
211 near surface (from the sounder instrument), we adopted the lower level in the present study as 950
212 hPa instead of sea surface / skin temperature. It was considered not appropriate to use SST/skin
213 temperature (though may be of higher accuracy) from a different source (like imager onboard the
214 same satellite) for estimating ΔT . It was felt that this will not give the advantage of the differencing
215 procedure employed earlier to detect inversion (Narayanan and Rao, 1981). This level criterion (950
216 – 850 hPa) was arrived at after a detailed examination of ΔT at a few more level intervals (viz 1000 –
217 900 hPa, 1000 – 850 hPa, etc).

218 Thus, we have used:

$$219 \quad \Delta T = T(950 \text{ hPa}) - T(850 \text{ hPa}) \quad (1)$$

220 to delineate MI. However, the actual levels used were 958 hPa and 852 hPa at which the support data
221 are available from the NOAA website.

222 While considering the normal atmospheric lapse rate of + 6 to +7 K / km (average of 340
223 non-inversion cases obtained during MONEX, figure not shown), it is expected to observe a ΔT of
224 + 6 to +7 K between 950 and 850 hPa (~ 1 km height difference). Note that Narayanan and Rao
225 (1981) have identified inversion (non-inversion) region as $\Delta T \leq + 2$ K ($\Delta T > + 2$ K) in TIROS – N
226 satellite data for a height range difference of ~ 0.75 km. For the present study (for 1 km height
227 difference) the same would translate to $\Delta T \sim + 2.7$ K for inversion delineation. However, to provide
228 margin of error, we have still considered $\Delta T \leq +2$ K as criterion of inversion region. The interval 2.0
229 K to 2.7 K may still be a grey region which could be interpreted as inversion region on some
230 occasions. The criterion of $\Delta T \geq + 4$ K as non – inversion regions has been adopted. In the example
231 shown in Fig. 1a, ΔT is (minus) - 1.3 K (note however, that the actual inversion value is ~ - 5 K
232 between surface and 900 hPa).

233 In general, a sudden drop in the water vapor just above the inversion is observed (e.g. RH
234 drop of ~ 70 %, as shown in Fig 1a). Since all the data sources mentioned in section 2 provide water
235 vapor information, we also have examined the changes happening in water vapor near/above the
236 inversion altitude. In general, inversion is identified in the temperature (water vapor) where it
237 increases (decreases sharply) instead of decreasing (decreasing gradually) with altitude. For
238 obtaining detailed characteristics of MIs over the Arabian sea, we have selected three $3^\circ \times 3^\circ$ grid
239 boxes centered at latitude 18.5° N, and located at longitudes 60° E as WAS, 64° E as CAS (central
240 AS), 71° E as EAS (as shown in Fig.3).

241 **3.1.Quality checks for the profiles and volume of data**

242 Each temperature profile from the satellite data was interpolated from surface to 500 hPa (26
243 levels of support data) at 0.25 km intervals for our preliminary analysis. We have used the quality
244 flag 0 and 1 from the given data set which are corresponding to best and good. There were many

245 erroneous profiles which could be observed even from a cursory examination of the data. Such bad
246 profiles are discarded. The temperatures at a few levels were far wide of the normal profile. To
247 account for these types of profiles, we applied a quality check to filter out spurious data. All profiles
248 of July and August months of 2009 (poor monsoon year) and 2011 (normal monsoon year) were
249 sorted out in 3 x 3 boxes of WAS and EAS. For each month the mean and standard deviation were
250 obtained for each interpolated levels separately. Those profiles for which the data at any one level
251 was lying beyond + / - 2 sigma of the mean, were not considered for further analysis. From this
252 procedure we saw that nearly 25 – 30 % of profiles were getting filtered out.

253 Using these quality checked profiles, the procedure for selecting the right levels for
254 calculating ΔT was established. Thereafter, for all the other monsoon days of the five years, we have
255 computed ΔT for individual profiles by an automated procedure (without resorting to examining each
256 profile). They were grouped and their ΔT values averaged in $1^\circ \times 1^\circ$ bins over the whole AS region.
257 Diurnal variation of ΔT was examined for a few months of data. Once we made sure that this is not
258 discernible, the day and night data of a calendar day were merged in $1^\circ \times 1^\circ$ boxes.

259 For further analysis, the average ΔT values for the day (24 hr period) at $1^\circ \times 1^\circ$ grids have
260 been used. Due to averaging of ΔT of all the profiles in $1^\circ \times 1^\circ$ box and morning and evening
261 overpasses (~ 6 to 8 values of ΔT in 24 hours), the strength of MI may be getting somewhat reduced
262 (as MI occur at slightly different levels within a vertical range of 25 - 50 hPa, for different profiles in
263 the same $1^\circ \times 1^\circ$ box). For some studies (e.g. for Fig 2, 4, 5, etc), we have used only a section of
264 these data sets. The total number of profiles considered for the five years amount to nearly half a
265 million, each for AIRS and IASI – considering that nearly 30 % profiles did not pass through our
266 quality check.

267

268

269

270 **4. Results and Discussions**

271 **4. 1. Monsoon Inversions observed in satellite and ERA-Interim datasets**

272 Fig. 1a and 1b show MI observed on 27 June 1979 at 0730 GMT at 20°N, 60°E through
273 MONEX radiosonde and ERA – Interim data, respectively. The detailed comparison study between
274 TIROS – N satellite data of 1979 and concurrent in-situ MONEX radiosonde profiles for 1979
275 southwest monsoon carried out by Narayanan and Rao (1981) is summarized in Table 2. This was
276 the only occasion (1979) when in-situ data were available over AS to compare with satellite
277 soundings. Thus, comparison of current satellite observations is being done in this study with ERA-
278 Interim data. In this case, ERA – Interim data also catches the inversion but with a less rise in
279 temperature (~ 3 - 4 K) and decrease in RH (~ 60%). To show the efficiency and strength of
280 currently available satellite measurements to delineate features of MI over AS, typical profiles of
281 temperature and RH obtained from collocated IASI and ERA-Interim on 30 July 2009, 0530 GMT
282 are plotted in Fig. 1c, and 1d, respectively. A clear MI in the satellite profile and ERA-Interim can be
283 noticed though with somewhat varying strengths and base of inversion height. However, the top
284 height of inversion is consistent. These are the first reported results of MI features seen directly from
285 the satellite observations over the AS which were shown earlier by Narayanan and Rao (1981) in an
286 indirect way by using ΔT indices. In general, in the individual satellite profiles, we are able to see the
287 MI strengths ranging from ~ + 2 to - 6 K (-8.8 K being the actual temperature difference between
288 930 hPa and 850 hPa in Fig. 1c). These MI lie mostly below 850 hPa level, but in rare occasions we
289 could see them even up to 700 hPa over the EAS – but of much weaker strength. The strength of MI
290 is also seen to be decreasing from WAS to EAS which will be discussed in detail in later sections.

291 Thus, in Fig. 1, we have seen examples of MI comparison between radiosonde and ERA
292 interim (1979) and between IASI and ERA-Interim (2009). There are some minor inconsistencies by
293 way of inversion heights in individual profiles of the three data sets. However, our objective here is

294 to examine the large scale characteristics of MI by considering average ΔT computed from individual
295 profiles in $1^\circ \times 1^\circ$ grids.

296 **4. 2. Contrasting behavior of MI between WAS and EAS**

297 As observed from Fig. 1, MI can lie between surface and ~ 2 km during Indian Summer
298 Monsoon (ISM) season (JJAS). Careful examination of time evolution of ΔT over the western
299 Arabian sea reveals that the MI appears around first half of May and dissipate around late
300 September. Fig. 2 shows the evolution of the MI during two contrasting years (2009 a poor monsoon
301 year and 2011 a normal monsoon year). During the peak monsoon season of July – August, the
302 difference in ΔT between the two years is significant. Also MI is more frequently observed with
303 higher strength during the peak monsoon months of July and August. To investigate further their
304 contrasting features in WAS and EAS, data only of July and August from 2009 to 2013 are
305 presented.

306 In Fig. 3 we have summarized the three important characteristics of MI: their base altitude,
307 strength (as revealed by ΔT) and percentage occurrence during the complete season. For brevity, the
308 results of only July and August months, averaged for all the five years 2009 – 2013 are shown in the
309 figures. Fig. 3a and 3b show the spatial variation of base altitude of MI during July and August,
310 respectively. The contrasting feature of base altitude of occurrence of MI is found mainly north of
311 15° N from the selected three grid boxes. It increases from WAS (below 1 km) to EAS (above 1.5
312 km) through CAS (1.0 -1.5 km).

313 As mentioned earlier, from very limited observations previous studies (Colon, 1964; Ramage,
314 1966; Narayanan and Rao, 2004) had suggested that strength and frequency of occurrence of the MI
315 days will be more over WAS than over EAS. To investigate this contrasting behavior of MI in detail
316 from satellite soundings, we examined the spatial variations of ΔT . Fig. 3c (July) and 3d (August)
317 shows the strength of MI increasing from EAS to the WAS and is prevalent mainly north of 15° N
318 latitude extending from 15° N to 25° N latitude and 55° E to 68° E longitude. The strength of MI can

319 be noticed as $\sim + 2$ K near Arabia coast, but the normal environmental lapse rate condition of + 6 to
320 + 7 K/km is restored towards the Indian coast. From these figures a clear contrast in ΔT with a
321 difference of around 2 K in the southeast quadrant of AS between July and August is also noticed. In
322 general, the AS is covered with lapse rate of + 4 K/km, which is the condition for taking the
323 atmosphere towards stability during the month of August. The Somali low level jet is the location of
324 permanent region of MI during the month of July. In the spatial distribution of monsoon low level jet
325 (Roja Raman et al. 2011) reveals that the center of the core is seen around 13°N and 60°E and exists
326 strong shear between 850 hpa and 700 hpa. Strong surface winds of south-west monsoon produce an
327 Ekman transport perpendicular to the wind flow with strong upwelling in the region which in turn
328 brings the cool water from the deeper layers to surface. Simon et al. (2007) showed that WAS region
329 is the region of Somali upwelling, and also since the low level jet and surface wind are of the order
330 of ~ 20 m/s, they produce sufficient cooling and the air above this region is still warmer when
331 compared to the upwelling area, producing strong inversion.

332 Fig. 3e and 3f show the spatial variation of percentage occurrence (PO) of MI during July and
333 August months. PO is calculated corresponding to $\Delta T \leq + 2$ K criteria. In general, it is observed that
334 WAS shows more number of MI cases (50 to 70%) compared to EAS (10 to 20%). ERA-Interim data
335 show only 30 to 50% cases of MI over WAS which will be dealt in detail in the following sub-
336 sections. The maximum PO during the four months of monsoon over the WAS are 40 % (June), 60
337 % (July), 50 % (August) and 30 % (September) (figure not shown). The areal extent of the maximum
338 PO is seen during July. During September, very small area of northern AS is covered with ~ 50 %.
339 No inversion is seen in the EAS box during the June and September periods. Despite its low strength
340 (ΔT) PO show maximum occurrence of 60% in July. Since the PO and strength of MI over the CAS
341 are in between the features of EAS and WAS, further discussions pertain, only to WAS and EAS
342 boxes.

343 The PO of ΔT values in different ranges observed in IASI for the five monsoon seasons is
344 shown in Fig. 4. ΔT values range from -2 to + 6 K (0 to + 7 K) in WAS (EAS) with peak occurring
345 around + 1 to + 2 K (+3 to +4 K). There are only a few values of ΔT less than + 2 K in EAS. Similar
346 analysis is also made using ERA-Interim data and is shown in bottom panels of Fig. 4. ERA-Interim
347 data show the contrast between WAS and EAS more clearly. In case of q at 700 hPa a difference of
348 about 2 g/kg can be noticed, with EAS having higher humidity values than WAS in IASI. However,
349 this feature is not observed in the ERA-Interim data.

350 To further examine the contrasting behavior between EAS and WAS, time series of ΔT and
351 water vapour at 700 hPa is considered for different years. Daily mean variations of ΔT and specific
352 humidity, q , at 700 hPa in WAS and EAS during the monsoon season of the year 2012 observed by
353 IASI is shown in Fig. 5. Note that we have included results of all the days irrespective of whether MI
354 is present or not. Three point average smoothed curves are shown in the respective panels. In
355 general, it can be seen that WAS ΔT (q at 700 hPa) values are $\sim + 2$ K (1 - 2 g/kg) less than those
356 over EAS for the season as a whole (Fig. 5a and 5b). During all the years (2009 - 2013) of the
357 present study, IASI reveals (figure not shown) this feature. Similar analysis has been carried out
358 using ERA-Interim reanalysis data and is shown in Fig. 5c and 5d. A clear contrast between WAS
359 and EAS in ΔT can be noticed in ERA-Interim data. A mean difference of ~ 2 K (~ 1 g/kg) can be
360 noticed in ΔT (q at 700 hPa) between WAS and EAS, with EAS values being lower. A cyclic
361 behavior in ΔT variations with a period of ~ 20 -25 days in case of ERA-Interim is noticed but not
362 observed in the satellite measurements. There exists no significant diurnal variation in ΔT (figure not
363 shown). This was verified before averaging ΔT of all profiles (day and night) in the $1^\circ \times 1^\circ$ grids.
364 Due to inversion and stability, moisture is getting trapped at lower levels over WAS compared to
365 EAS as indicated in Fig. 5b and 5d observed from IASI and ERA-Interim, respectively.

366

367

368 **4.3. Relation between MI over AS and monsoon activity**

369 Past investigations (e.g. Gadgil and Joseph, 2003) showed that the monsoon features vary
370 with activity of the monsoon. In general during the active phase of the ISM, there will be more
371 precipitation over central India (18°-28°N and 65° to 88°E). Similar variations in precipitation during
372 the monsoon season can also be expected on regional scales. Gadgil and Joseph (2003), Kripalani et
373 al. (2004), Rajeevan et al. (2006) have considered the daily rainfall time series over central India
374 during monsoon months along with the climate normal to delineate ‘active’ and ‘break’ periods over
375 the Indian region. On the basis of this data, Rajeevan and Bhate (2009) have defined active and break
376 phases over central India by considering the days exceeding the climate mean with +1 (-1)
377 standardized anomaly as active (break) periods, provided it should persist at least for 3 days (triad).

378 Fig. 6 shows the latitude - longitude cross section of ΔT and q at 700 hPa for active (14 - 17
379 July 2009) and break (30 July - 11 Aug. 2009) spells for the monsoon season of 2009 observed using
380 IASI and ERA-Interim data. Irrespective of the data source, ΔT and associated q at 700 hPa reveal
381 that a large part of WAS is covered with MI ($\Delta T \leq +2$ K and less moisture values) up to west of ~
382 68° E during the break spell as seen in Fig. 6a and 6e. In the north AS, MI reach as close as Gujarat
383 coast during break spells (especially in ERA-Interim data), but are restricted to WAS during active
384 spells. During the active spell, the inversion regions from ΔT maps are discontinuous west of 65° E in
385 Fig. 6c. Also strengths of ΔT in WAS are more as observed by ERA-Interim than by IASI during
386 break spells (30 July – 11 August 2009). ERA-Interim show (Fig. 6e and 6g) more smoothed results
387 and there is less change in areal extent in this case. Specific humidity q at 700 hPa shows clear result
388 that during the break spell AS has less moisture and more during the active spell. One can notice the
389 feature of inversion from the figure where water vapor is being trapped in the lower portion resulting
390 in less moisture over WAS and more over the EAS. Thus, the q values also give a good indication of
391 the inversion feature.

392

393 **4.4. MI during normal and poor monsoon years**

394 It is well known that strong MI suppresses the vertical development of clouds; rain cannot
395 occur in such situations (Sathiyamoorthy et al., 2013). Using ARMEX-I (2002) data, Bhat (2006)
396 could notice strong and persistent inversions in the atmosphere over the AS and west coast of India.
397 This data proved very valuable as July 2002 rainfall was the lowest in the recorded history and the
398 data collected over the AS and on the west coast helped in understanding the conditions that
399 prevailed over the eastern AS during one of the worst monsoon years. The relation between MI and
400 central India rainfall is further investigated by separating the MI observed during normal (2010 -
401 2013) and poor monsoon (2009) years. Time variations of ΔT observed over WAS during two
402 contrasting years of 2009 and 2011 obtained from IASI measurements and ERA-Interim data are
403 shown in Fig. 7. It can be seen that good monsoon year 2011 has higher ΔT than poor monsoon year
404 2009 (Fig. 7a), and is the same for q i.e. higher value for the year 2011 (Fig. 7b). ΔT is observed to
405 be lower by about 2 K during the season as a whole in the poor monsoon year when compared to the
406 good monsoon year, suggesting the possibility of a variation of this parameter between normal and
407 poor monsoon years. This aspect is clear from the right panels where difference between 2011 and
408 2009 observed in ΔT (Fig. 7c) and q at 700 hPa (Fig. 7d) are shown. From this figure we can infer
409 that the year 2009 has less value of ΔT and less value for q suggesting stronger MI during poor
410 monsoon year. Note that during most of the time, the temperature in 2011 is higher (the difference
411 between 2011 and 2009 showing positive values) and less temperature lapse rate means more stable
412 layered atmosphere. In 2011, WAS temperature show higher values revealing less MI over AS when
413 compared to 2009. The decreasing trend in ΔT is discernible in difference plots for some particular
414 epochs. In general, ERA-Interim also show these features (Fig. 7e and 7f), but only to a moderate
415 extent. It may be noted that these inferences are based on the results of only one poor monsoon year
416 (2009).

417

418 **4.5. Inter-comparison of MI features with IASI, AIRS and ERA**

419 Inter-comparison of the gross features of PO of MI (with $\Delta T \leq 2$ K) in WAS and EAS
420 estimated for the five years of monsoon season by IASI, AIRS and ERA-Interim data are shown in
421 Fig. 8. In general, when we consider ΔT as a parameter to detect MI, clear contrasting feature
422 between WAS and EAS with higher PO in WAS can be noticed in all the data sources mentioned
423 above. PO in the IASI measurements ranges from 23% to 54%. Among these data sets, ERA-Interim
424 shows huge difference in the percentage occurrences between WAS and EAS, to the extent that not
425 even a single MI is seen in EAS in any year. Since the vertical resolution of the IASI temperature
426 profiles is better than AIRS, higher PO of MI in the WAS is noticed throughout when compared to
427 AIRS, except in the case of 2012. However, ERA- Interim being a combination of model and
428 observations, it is not able to pick up the MI in the EAS where the strength of inversion is also
429 weak. The model appears to be smoothening the MI features of IASI when it is assimilated in the
430 ERA – Interim.

431 Among the satellite observations, IASI shows higher PO of MI days than AIRS, except
432 during 2012 over WAS. A distinct contrast between WAS and EAS with higher PO in the former
433 region can be noticed. When we consider EAS as a place to detect MI, AIRS observed always higher
434 PO than IASI and almost nothing is noticed in ERA-Interim. Thus, we may infer that IASI is
435 performing better than AIRS for detecting MI (as ERA is in better agreement with IASI rather than
436 with AIRS). Note that large inter-annual variability in MI is observed and this is expected to reflect
437 in the monsoonal activity over Indian region. It can also be seen that there is a steady decrease of PO
438 of MI as observed by IASI from 2009 to 2013. No such feature is observed in AIRS – which shows
439 more random behavior over the different years.

440 We have also analysed and compared the ΔT observed by IASI and AIRS over WAS and
441 EAS (figure not shown). The analysis suggests that these two data sets cannot be merged to study
442 the small changes of ΔT in their intra-seasonal and inter-annual variations. This and the other

443 differences related to q at 700 hPa constrained us not to combine the AIRS data with IASI data in the
444 present study.

445 **4.6. Monsoon Inversion derived from other parameters**

446 Narayanan and Rao (1989) had also considered equivalent potential temperature (θ_e)
447 differences to study MI. θ_e incorporates the effect of both temperature and humidity. However, the
448 dynamic range of $\Delta\theta_e$ is no better than that of ΔT . Recall that the troposphere is statically stable on
449 average, with a potential temperature gradient of 3.3 K/km (Wallace et. al., 2006). We make use of
450 another index here i.e. atmospheric refractivity (N) for identifying MI. Similar to θ_e , Refractivity
451 (N), is another atmospheric parameter which is a function of temperature and water vapor. It was
452 shown that better information on boundary layer can be obtained from refractivity profiles than
453 virtual potential temperature though both have temperature and water vapor information (Basha and
454 Ratnam, 2009). Refractivity, N has a higher dynamic range and vertical variation as compared to
455 temperature (~ 15 N units vis a vis 2 K). More advantage of using N for delineating MI will be
456 available, provided, it is measured directly, for example, using GPS Radio Occultation technique,
457 instead of computing it from temperature and water vapor obtained from the sounders or from
458 radiosonde. However, the spatio-temporal density of direct N observations is too sparse to get
459 meaningful statistics over equatorial regions.

460 We have computed refractivity N , from temperature and water vapor data of IASI (and
461 MONEX radiosonde data), given by the expression:

$$462 \quad N = 77.6 \left(\frac{P}{T} \right) + 3.73 \times 10^5 \left(\frac{e}{T^2} \right) \quad (2)$$

463 where P is pressure, T temperature and e water vapor pressure.

464 Similar to ΔT we have defined an index ' ΔN ' as:

$$465 \quad \Delta N = N(950 \text{ hPa}) - N(850 \text{ hPa}) \quad (3)$$

466 Profile of N computed from the temperature and humidity profiles of dropsonde (Fig. 9a) of
467 MONEX time is shown in Fig. 9b. A drastic decrease in N (by 129 N units between 950 and 850
468 hPa) can be noticed near MI altitudes in this example. Thus, N can also be taken as a potential
469 parameter to delineate inversion and for studying spatial and temporal variations of MI.

470 In order to see the relation between ΔT and ΔN , we have estimated ΔN using all the MONEX
471 profiles obtained over AS. These include both inversion and non-inversion cases. There were 32
472 (346) profiles with inversion (non- inversion). Note that $\Delta T \leq + 2$ K and $\Delta T > + 4$ K are only
473 considered for obtaining above statistics and there exists 34 profiles in the transition zone (+ 2 to + 3
474 K). Scatter plot between ΔT and ΔN for all 411 in-situ profiles of MONEX over AS is shown in Fig.
475 9c. Correlation coefficients between the two parameters are found to be 0.56 with 15.7 as standard
476 deviation. Note that $\Delta T \leq + 2$ K (inversion region) corresponds to $\Delta N > 50$ N units which is shown
477 as blue line in Fig. 9c. We can infer that if ΔN is less than 50 N units it corresponds to non-inversion
478 region (ΔN more than 50 may be inversion or otherwise). ΔN is thus a supportive parameter to ΔT in
479 identifying inversion / non inversion. Because of its larger dynamic range, details of inversion have
480 been identified in the ΔT and ΔN maps (figure not shown).

481 It is well known that COSMIC satellites are able to provide N profiles directly. The spatial
482 and temporal sampling of COSMIC at any particular region are, however, very meager. The
483 comparison map of ΔN from IASI and ΔN from COSMIC combined for a long break spell from 30
484 July to 11 August 2009 has been studied. This long period accumulation of data was necessary to
485 have sufficient data points from COSMIC to cover the entire AS. One can see ΔN values above 50 N
486 units (inversion region) covering the entire Arabian sea corresponding to ΔT values being below 2 K
487 (shown by IASI, figure not shown). Over the AS region ΔN observed for all the five years of our
488 study were combined to produce the frequency distribution of ΔN over Western AS (5 – 25 °N, 56 –
489 65 °E, excluding land) and Eastern AS (5 – 25 °N, 66 – 75 °E, excluding land) and is shown in Fig
490 10. Over WAS, 712 cases and over EAS 547 cases are showing $\Delta N > 50$ N units (which may be

491 supportive to inversion). A difference of about 10 N units can be noticed, with WAS having higher
492 ΔN values.

493 **5. Summary and Conclusions**

494 Low level MI characteristics, which usually occur below 700 hPa over the AS during
495 southwest monsoon months, have been identified directly from operational satellite temperature
496 retrievals. For the first time we have shown here cases of direct and unambiguous delineation of MI
497 from the satellite temperature and water vapor retrieval observations. We have used five years (2009-
498 2013) data of two different satellite sounder instruments (mainly from IASI and for inter comparison
499 AIRS) along with ERA-Interim reanalysis data to delineate the characteristics of MI over AS. Their
500 percentage occurrence, base height and strength have been studied. For supporting our findings, we
501 also compare with the campaign of MONEX 1979 in-situ measurements over AS. The main findings
502 obtained from the observational study are summarized in the following:

- 503 1. Percentage occurrences of MI over WAS (up to $\sim 65^\circ\text{E}$) is $\sim 60 - 70\%$ and are always higher
504 and stronger than over EAS. WAS ΔT values are $\sim 2\text{ K}$ less than those over EAS.
- 505 2. MI is stronger during poor monsoon year (2009) and occurs on more occasions in WAS
506 during break spells (30 July – 11 August 2009). Whether this is true or not for all poor
507 monsoon years need to be checked with more years of data.
- 508 3. These features are also observed in the ERA-Interim data, but are restricted to some parts of
509 AS with more smoothed variability.
- 510 4. Inter-comparison of IASI and AIRS profiles from the view of study of inversion suggests the
511 differences do not warrant a mix of these two data sets for this study.
- 512 5. The refractivity data has only a supporting role to identify monsoon inversion regions.

513 Thus, MI seems to be a semi-permanent feature of Indian summer monsoon. It is suggested to
514 include this feature also in future monsoon diagnostic and forecast studies. The diagnostics from
515 ERA-Interim suggest the possibility of AS MI getting formed during mid May, primarily due to

516 subsidence mechanism and maintained later by the combined effects of advection and subsidence
517 which is the subject of our future study.

518

519 **Acknowledgments:** This work is a part of the INSAT – 3D project sponsored by the Indian Space
520 Research Organization (ISRO), for which we are thankful to Space Applications Centre,
521 Ahmadabad. We wish to thank C. M. Kishtawal, V. Sathiyamoorthy, S. Ghouse Basha, Jyotirmayee
522 and Ranjit Thapa for discussions and for help in data processing aspects and help in using HPCC.
523 The authors would like to thank ECMWF (<http://apps.ecmwf.int/datasets>) for providing data of ERA-
524 Interim, GESDISC(<http://mirador.gsfc.nasa.gov/>)for AIRS, NOAA
525 (<http://www.nsof.class.noaa.gov/>for IASI) for IASI through ftp. We also thank IMD for providing
526 rainfall data over Indian land mass.

527 **References**

- 528 Anthes, R. A., Bernhardt, P. A., Chen, Y., Cucurull, L., Dymond, K. F., Ector, D., Healy, S. B., Ho, S. P.,
529 Hunt, D. C., and Kuo, Y. H.: The COSMIC/FORMOSAT-3 mission: Early results, *Bul. Am.*
530 *Meteorol. Soc.*, 89, doi: 10.1175,1–21, 2008.
- 531 Basha, G. and Ratnam, M. V.: Identification of atmospheric boundary layer height over a
532 tropical station using high-resolution radiosonde refractivity profiles: Comparison with GPS radio
533 occultation measurements, *J. Geophys. Res.*, 114, D16101, doi:10.1029/2008JD011692, 2009.
- 534 Bhat, G. S.: The Indian drought of 2002: a sub-seasonal phenomenon, *Q. J. Roy. Meteor. Soc.*, 32,
535 2583-2602, 2006.
- 536 Clerbaux, C., Hadji-Lazaro, J., Turquety, S., George, M., Coheur, P. F., Hurtmans, D., Wespes, C., Herbin,
537 H., Blumstein, D., and Tourniers, B.: The IASI/MetOp mission: First observations and highlights of its
538 potential contribution to GMES, *COSPAR Inf. Bul.*, 19–24, 2007.
- 539 Clerbaux, C., Boynard, A., Clarisse, L., George, M., Hadji-Lazaro, J., Herbin, H., Hurtmans, D., Pommier,
540 M., Razavi, A., and Turquety, S.: Monitoring of atmospheric composition using the thermal infrared
541 IASI/MetOp sounder, *Atmos. Chem. Phys.*, 9, 6041–6054, 2009.
- 542 Colon, J. A.: On interactions between the Southwest Monsoon Current and the Sea Surface over the
543 Arabian Sea, *Indian J. Met. Geophys.*, 15, 183 – 200, 1964.
- 544 Das, P. K.: *The Monsoons*, Nation Book Trust, New Delhi, India, ISBN 978-81-237-1123-2, 193,
545 2002.
- 546 Dwivedi, S., Sathiyamoorthy, V., Narayanan, M. S., and Rao, D. N.: A Study on the Lower
547 Tropospheric Thermal Inversion Over the Arabian Sea Using Radiosonde and IASI Data, *IEEE*
548 *Journal of Selected Topics in Applied Earth Observations and Remote Sensing*, 9, 490-495, doi:
549 10.1109/JSTARS.2015.2506759, 2016.
- 550 Gadgil, S., and Joseph, P. V.: On breaks of the Indian monsoon, *Proc. Indian Acad. Sci.*, 112, 529–
551 558, 2003.

552 Kidder, S. Q., and Haar, T. H.V., Academic press inc., California, U.S.A.: Satellite Meteorology -
553 An Introduction, ISBN 0-12-406430-2,199, 1995.

554 Kripalani, R. H., Kulkarni, S. A., Sabade, S., Revadekar, J. V., Patwardhan, S. K., and Kulkarni, J.
555 R.: Intra-seasonal oscillations during monsoon 2002 and 2003, *Curr. Sci.*, 87, 325– 331, 2004.

556 Kwon, E.H., Sohn, B. J., William, L., and Smith, J. L.: Validating IASI temperature and moisture
557 sounding retrievals over East Asia using radiosonde observations, *J. Atmos. Oceanic Technol.*, 29,
558 1250–1262, doi:10.1175/JTECH-D-11-00078.1, 2012.

559 Kursinski, E. R., Hajj, G. A., Schofield, J. T., Linfield, R. P. and Hardy, K. R.: Observing Earth’s
560 atmosphere with radio occultation measurements using the Global Positioning System, *J. Geophys.*
561 *Res.*, 102, 23,429–23,466, doi:10.1029/97JD01569, 1997.

562 Lambrigtsen, B. H.: Calibration of the AIRS microwave instruments, *IEEE Trans. Geosci. Remote*
563 *Sens.*, 41, 369–378, 2003.

564 Narayanan, M. S., and Rao, B. M.: Detection of monsoon inversion by TIROS-N satellite, *Nature*,
565 294, 546 – 548, 1981.

566 Narayanan, M. S., and Rao, B. M.: Stratification and convection over Arabian Sea during monsoon
567 1979 from satellite data, *Proc. Indian Acad. Sci. (Earth Planet. Sci.)*, 98, 4, 339-352, 1989.

568 Narayanan, M. S., Rao, B.M. , Shah, S., Prasad, V. S., and Bhat, G.S.: Role of atmospheric stability
569 over the Arabian Sea and the unprecedented failure of monsoon 2002, *Curr. Sci.*, 86, 7, 938 – 947,
570 2004.

571 Rajeevan, M., and Bhate, J.: A high resolution daily gridded rainfall data set (1971–2005) for
572 mesoscale meteorological studies, *Curr. Sci.*, 96, 558– 562, 2009.

573 Rajeevan, M., Bhate, J., Kale, J. D., and Lal, B.: High resolution daily gridded rainfall data for the
574 Indian region: Analysis of break and active monsoon spells, *Curr. Sci.*, 91, 296– 306, 2006.

575 Ramage, C. S.: The Summer Atmospheric Circulation over the Arabian Sea, *J. Atmos. Sci.*, 23, 144
576 – 150, 1966.

577 Roja Raman, M., Venkat Ratnam, M., Rajeevan, M., Jagannadha Rao, V.V.M., and Vijaya Bhaskara
578 Rao, S.: Intriguing aspects of monsoon low level jet over peninsular India revealed by high-
579 resolution GPS radiosonde observations, *J. Atmos. Sci.*, 68, 1413-1423, doi:
580 10.1175/2011JAS3611.1, 2011.

581 Sathiyamoorthy, V., Mahesh, C., Gopalan, K., Prakash, S., Shukla, B. P. and Mathur, A. K.:
582 Characteristics of low clouds over the Arabian Sea, *J. Geophys. Res.*, 118, 24, 13,489–13,503,
583 2013.

584 Schlüssel, P., Hultberg, T. H., Philipps, P. L., August, T., and Calbet, X.: The operational IASI level
585 2 processor, *Adv. Space Res.*, 36, 982–988, doi:10.1016/j.asr.2005.03.008, 2005.

586 Simmons, A. J., and Hollingsworth A.: Some aspects of the improvement in skill of numerical
587 prediction, *Q. J. R. Meteor. Soc.*, 128, 647–677, 2002.

588 Simmons, A., Uppala, S., and Dee, D.: Update on ERA-Interim, *ECMWF News l.*, 111, 5, 2007.

589 Simon, B., Rahman, S. H., Joshi, P. C. and Desai, P. S.: Shifting of the convective heat source over
590 the Indian Ocean region in relation to performance of monsoon: a satellite perspective, *Inter. J. of*
591 *Rem. Sens.*, 29:2, 387 – 397, doi: 10.1080/01431160701271966, 2007.

592 Smith, N., Smith Sr., W. L., Weisz, E., and Revercomb, H. E.: AIRS, IASI, and CrIS Retrieval Records at
593 Climate Scales: An Investigation into the Propagation of Systematic Uncertainty, *Am. Meteorol.*
594 *Soc.*, 54, 1565 – 1481, doi: 10.1175/JAMC-D-14-0299.1, 2015.

595 Susskind, J., Barnet, C. D., and Blaisdell, J.M.: Retrieval of atmospheric and surface parameters
596 from AIRS/AMSU/HSB data in the presence of clouds, *IEEE Trans. Geosci. Rem. Sem.*, 41, 390-
597 409, 2003.

598 Thomas W. S.: An assessment of Operational TIROS – N Temperature Retrievals over the United
599 States, *Monthly Weather Review*, *Am. Meteorol. Soc.*, 109, 110-119, 1981.

600 Wallace, J. M. and Hobbs, P. V., *International Geophysics series: Atmospheric Science - An*
601 *Introductory Survey*, Second Edition, 92, ISBN 13: 978-0-12-732951-2, 2006,.

602 WMO, GARP Publication series no.18,The Monsoon Experiment, 1976.

603

604

605

606

607

608

609 **Figure captions:**

610 **Figure 1.** Typical examples showing MI in T and RH on (a) 27 June 1979 at 0730 GMT at 20°N,
611 60°E measured by radiosonde during MONEX experiment, (b) same as (a) but at 0600 GMT from
612 ERA, (c) 30 July 2009 at 0514 GMT at 22°N, 68°E by IASI, (d) 30 July 2009 by ERA-Interim at
613 same location but at 0600 GMT. Note that scale for RH is shown in the top axis of (a) and (b).

614 **Figure 2.** Time series of ΔT for starting and ending of MI from April to October 2009 (black) and
615 2011 (blue). Green vertical lines are showing starting (01 May 2009) and ending (07 October 2009)
616 time for MI.

617 **Figure 3.** Base altitude occurrence of MI during (a) July, (b) August, ΔT (Strength) of MI (c) July,
618 (d) August, and Percentage occurrence of MI days (e) July, (f) August, averaged during 2009-2013
619 observed by IASI (We are selecting WAS, CAS and EAS from this figure).

620 **Figure 4.** Percentage occurrence of (a) ΔT and (b) q at 700 hPa observed in WAS and EAS during
621 monsoon season of the years 2009-2013 for various ranges of ΔT and q at 700 hPa by IASI. (c) and
622 (d) same as (a) and (b) but obtained from ERA-Interim data.

623 **Figure 5.** Time series of (a) ΔT and (b) q at 700 hPa observed over WAS and EAS grid boxes
624 during the monsoon season of the year 2012 by IASI, (c) and (d) same as (a) and (b) but obtained
625 using ERA – Interim data. 3-point smoothed curves are shown.

626 **Figure 6.** MI observed in (a) ΔT and (b) q at 700 hPa during break spells (30 July – 11 August 2009)
627 of the year 2009 by IASI, (c) and (d) same as (a) and (b) but observed during active spells (14-17
628 July 2009). (e) and (f) and (g) and (h), same as (a) and (b) and (c) and (d) but observed by ERA-
629 Interim, respectively.

630 **Figure 7.** Time variations of (a) ΔT and (b) q at 700 hPa observed over WAS during two contrasting
631 years of 2009 and 2011 by using IASI measurements and ERA-Interim products (e and f).
632 Difference between 2011 and 2009 observed in (c) ΔT and (d) q at 700 hPa for IASI and ERA-
633 Interim products (g and h).

634 **Figure 8.** Percentage occurrence of MI observed with (a) $\Delta T \leq 2K$ using IASI, AIRS and ERA-
635 Interim data during monsoon seasons of 2009-2013 over WAS and EAS.

636 **Figure 9.** Typical examples showing MI in temperature and RH on (a) 27 June 1979 at 0656 GMT at
637 $20^{\circ}N$, $62^{\circ}E$ obtained from dropsondes from MONEX experiment, (b) N profile (c) Scatter plot of
638 ΔT and ΔN .

639 **Figure 10.** Frequency of ΔN observed in Western AS and Eastern AS during monsoon season of the
640 years 2009-2013 for various ranges of ΔN by COSMIC. Western AS is showing higher
641 values means inversion is there.

642

643 **Table captions:**

644 **Table 1:** Data details for accuracy/error and availability.

645 **Table 2:** Comparison of aircraft profiles with satellite data.

646 **Table 1:** Data details for accuracy/error and availability.

	IASI	AIRS	COSMIC GPS - RO	ERA-Interim	MONEX 1979 In-situ data
Launch of satellite	MetOp – A launched in October 2006, 8461 spectral Channels	Aqua launched in May 2002, 2378 spectral channels	GPS – RO microsatellite receiver launched in April 2006	---	May – August 1979
Data availability from	August 2008	2003	April 2006	1979	May – August 1979
Data used in the present study	June – September 2009 - 2013	June – September 2009 – 2013	June – September 2009 - 2013	June – September 2009 - 2013	May – August 1979
Accuracy in Temperature	~ 1 K(RMS) at a vertical resolution of 1 Km(Clerbaux et al., 2007; 2009)	~ 1 K at a vertical resolution of 1 Km(Susskind et al., 2003)	Generally ~ 100m in the lower troposphere (not for T)	0.5 – 1.0 K at a vertical resolution of 0.8 – 1.0 km	± 1 °C in 4 vertical levels resolution(WMO report)
Accuracy in Humidity	~10 – 15 % accuracy with a 1 – 2 Km vertical resolution(Clerbaux et al., 2007; 2009)(Schlüssel et al., 2005)	~15 % accuracy with a 2 Km vertical layer resolution(Susskind et al., 2003)	---	~7.0 – 20 % at a vertical resolution of 0.8 – 1.0 km	± 30 % at a vertical resolution of 4 levels.
Accuracy in Refractivity	---	---	400 m to 1.4 km (Kursinski et al., 1997),		
Horizontal resolution	15 Km	25 Km	2000 soundings per day	1.5° x 1.5° (~ 80 km)	500 km
Pressure levels	1100- 0.0161 hPa - 100	1100 – 0.0161 hPa – 100	70% of occultations penetrate below 1 km (Anthes et al., 2008)	1013 – 1 hPa 37	1000 – 294 Different -2
Local equator crossing time	0930 LT descending node	1330 LT ascending node	-----	----	---
Swath	2200 km	1650 Km	-----		

647

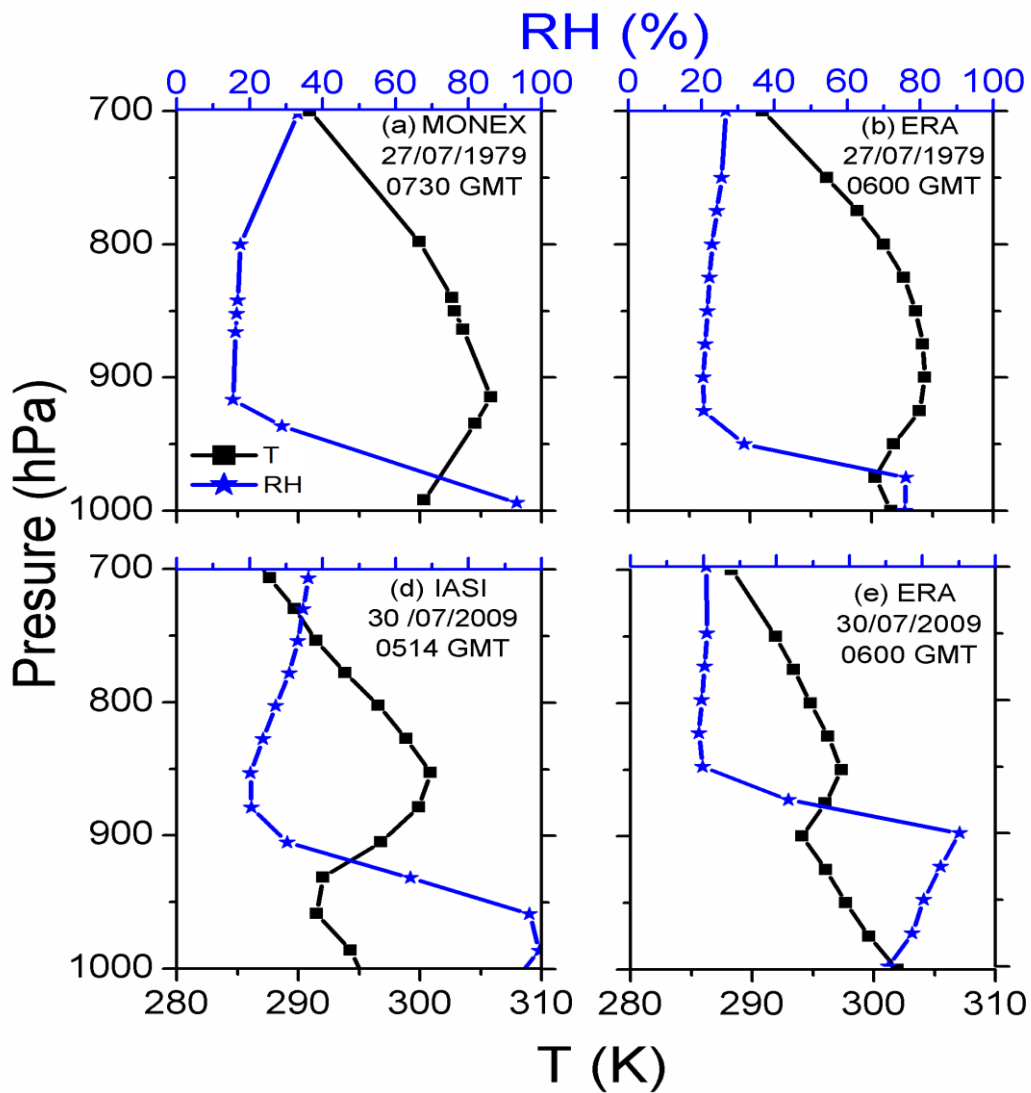
648

649 **Table 2:** Comparison of aircraft profiles with satellite data.

	Aircraft profiles	Near simultaneous satellite data	
		$\Delta T \leq 2^{\circ}\text{C}$	$\Delta T \geq 3^{\circ}\text{C}$
No. Of profiles with well – marked inversion below 850 mbar	30	23	7 (for four of them $\Delta T = 3^{\circ}\text{C}$)
No. Of profiles without well – marked inversion	129	0	129

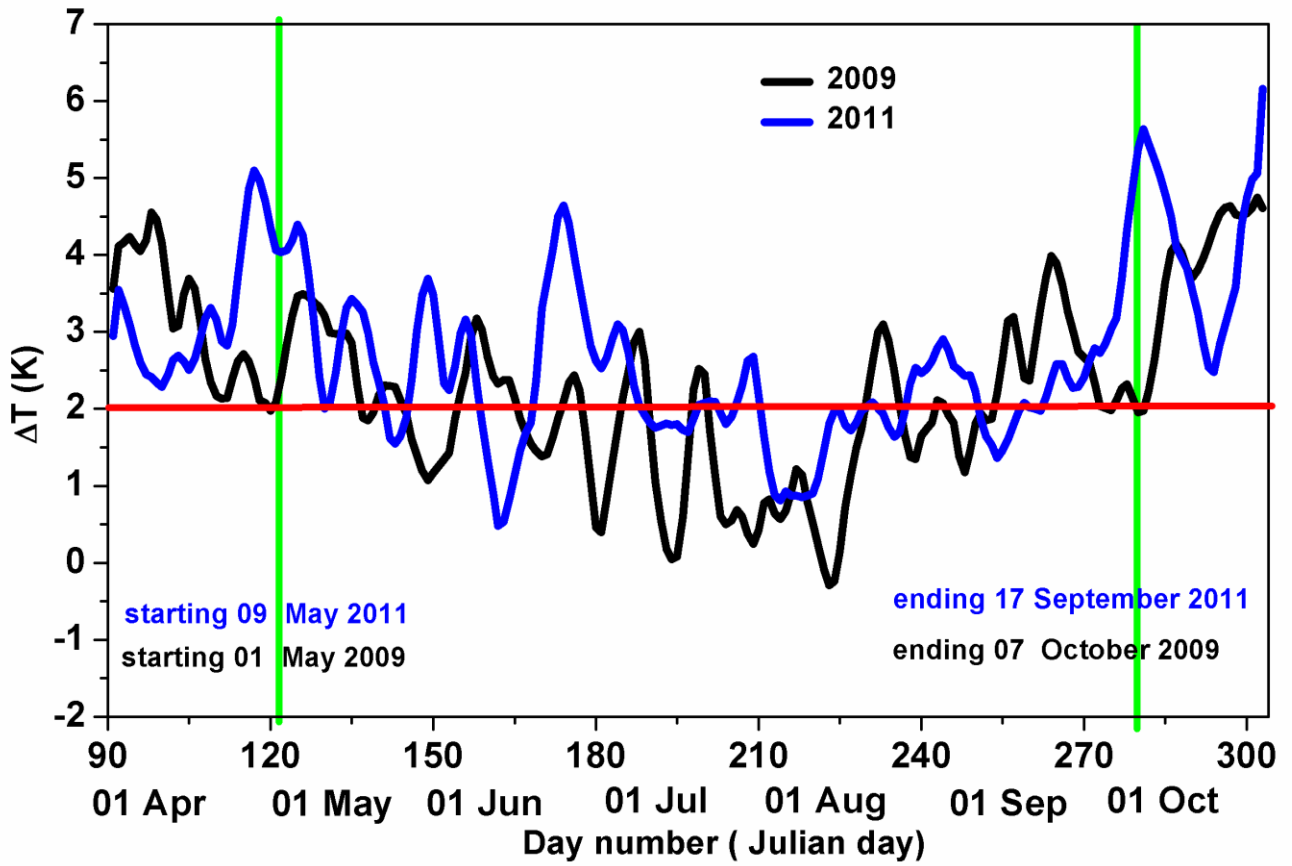
650 (Regenerated from Narayanan et al., 1981)

651



653

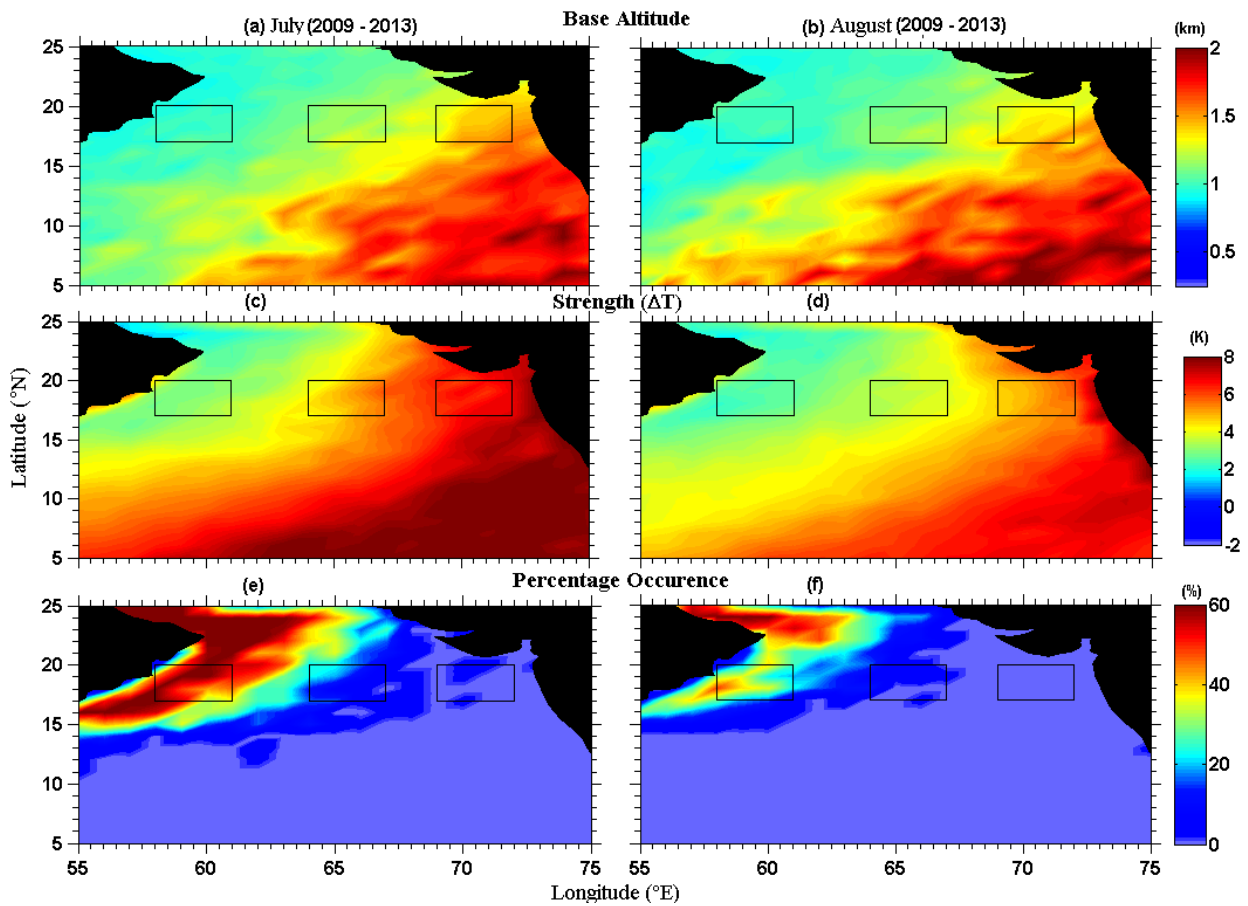
654 **Figure 1.** Typical examples showing MI in T and RH on (a) 27 June 1979 at 0730 GMT at 20°N,
 655 60°E measured by radiosonde during MONEX experiment, (b) same as (a) but at 0600 GMT from
 656 ERA, (c) 30 July 2009 at 0514 GMT at 22°N, 68°E by IASI, (d) 30 July 2009 by ERA-Interim at
 657 same location but at 0600 GMT. Note that scale for RH is shown in the top axis of (a) and (b).



658

659 **Figure 2.** Time series of ΔT for starting and ending of MI from April to October 2009 (black) and
 660 2011 (blue). Green vertical lines are showing starting (01 May 2009) and ending (07 October 2009)
 661 time for MI.

662



663

664

665

666

667

668

669

670

671

672

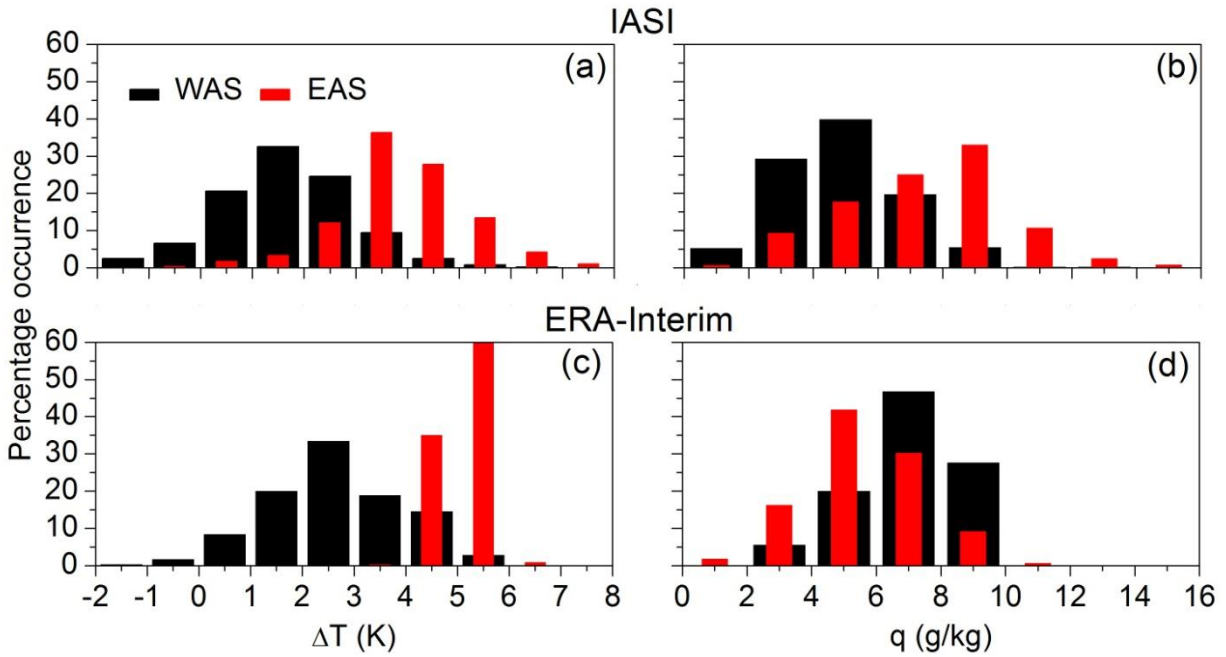
673

674

675

676

Figure 3. Base altitude occurrence of MI during (a) July, (b) August, ΔT (Strength) of MI (c) July, (d) August, and Percentage occurrence of MI days (e) July, (f) August, averaged during 2009-2013 observed by IASI (We are selecting WAS, CAS and EAS from this figure).



678

679 **Figure 4.** Percentage occurrence of (a) ΔT and (b) q at 700 hPa observed in WAS and EAS during
 680 monsoon season of the years 2009-2013 for various ranges of ΔT and q at 700 hPa by IASI. (c) and
 681 (d) same as (a) and (b) but obtained from ERA-Interim data.

682

683

684

685

686

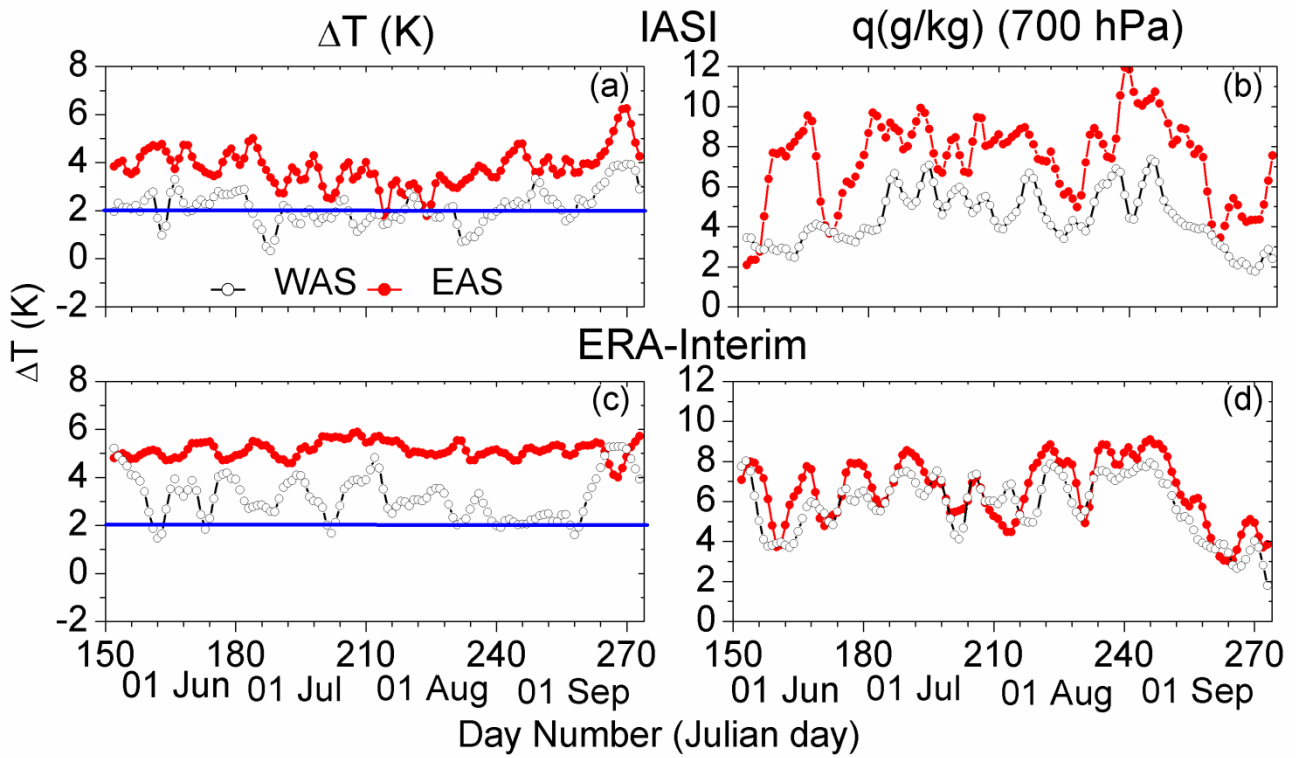
687

688

689

690

691



692

693 **Figure 5.** Time series of (a) ΔT and (b) q at 700 hPa observed over WAS and EAS grid boxes
 694 during the monsoon season of the year 2012 by IASI, (c) and (d) same as (a) and (b) but obtained
 695 using ERA – Interim data. 3-point smoothed curves are shown.

696

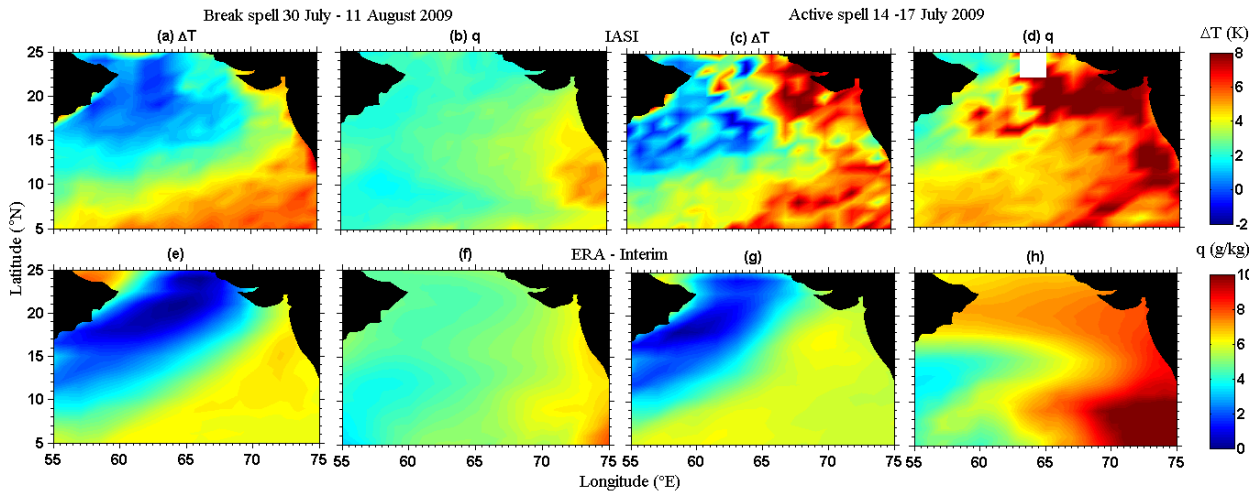
697

698

699

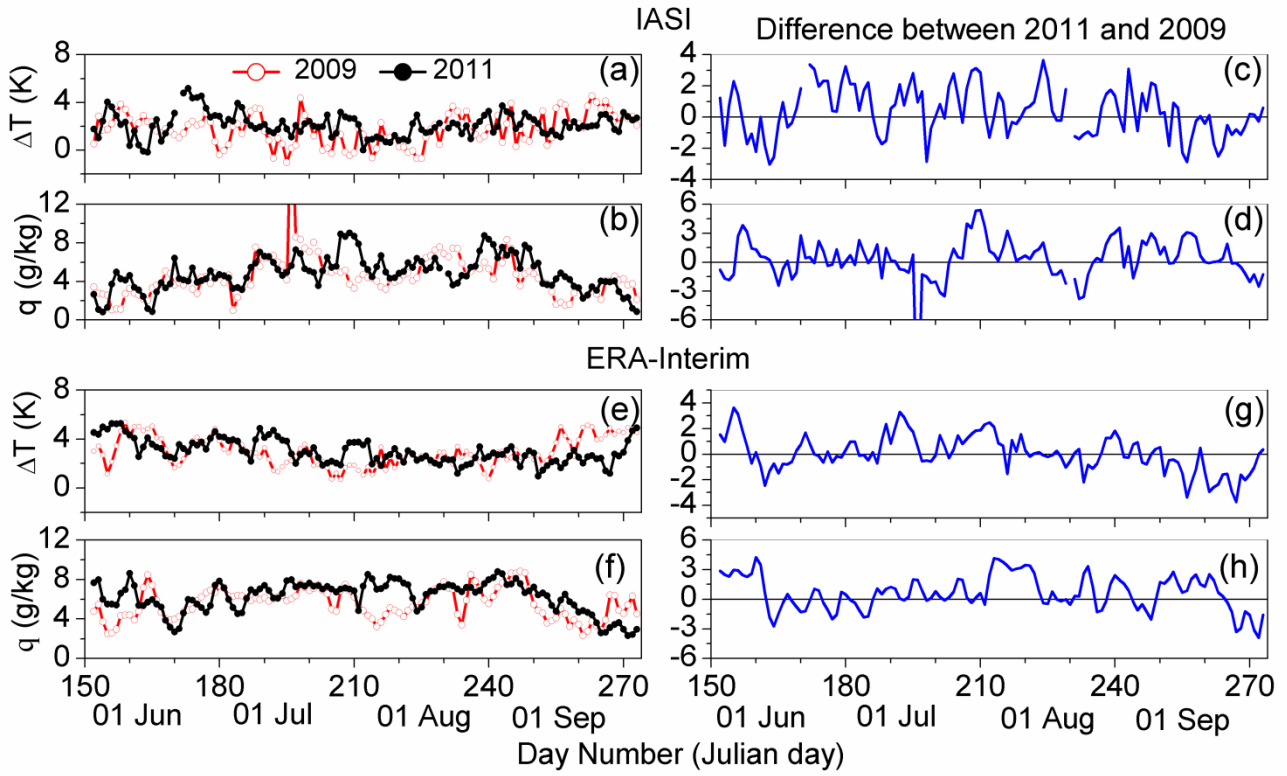
700

701



702
 703 **Figure 6.** MI observed in (a) ΔT and (b) q at 700 hPa during break spells (30 July – 11 August
 704 2009) of the year 2009 by IASI, (c) and (d) same as (a) and (b) but observed during active spells
 705 (14-17 July 2009). (e) and (f) and (g) and (h), same as (a) and (b) and (c) and (d) but observed by
 706 ERA-Interim, respectively.

707
 708
 709
 710
 711
 712
 713
 714
 715



716

717 **Figure 7.** Time variations of (a) ΔT and (b) q at 700 hPa observed over WAS during two contrasting
 718 years of 2009 and 2011 by using IASI measurements and ERA-Interim products (e and f).
 719 Difference between 2011 and 2009 observed in (c) ΔT and (d) q at 700 hPa for IASI and ERA-
 720 Interim products (g and h).

721

722

723

724

725

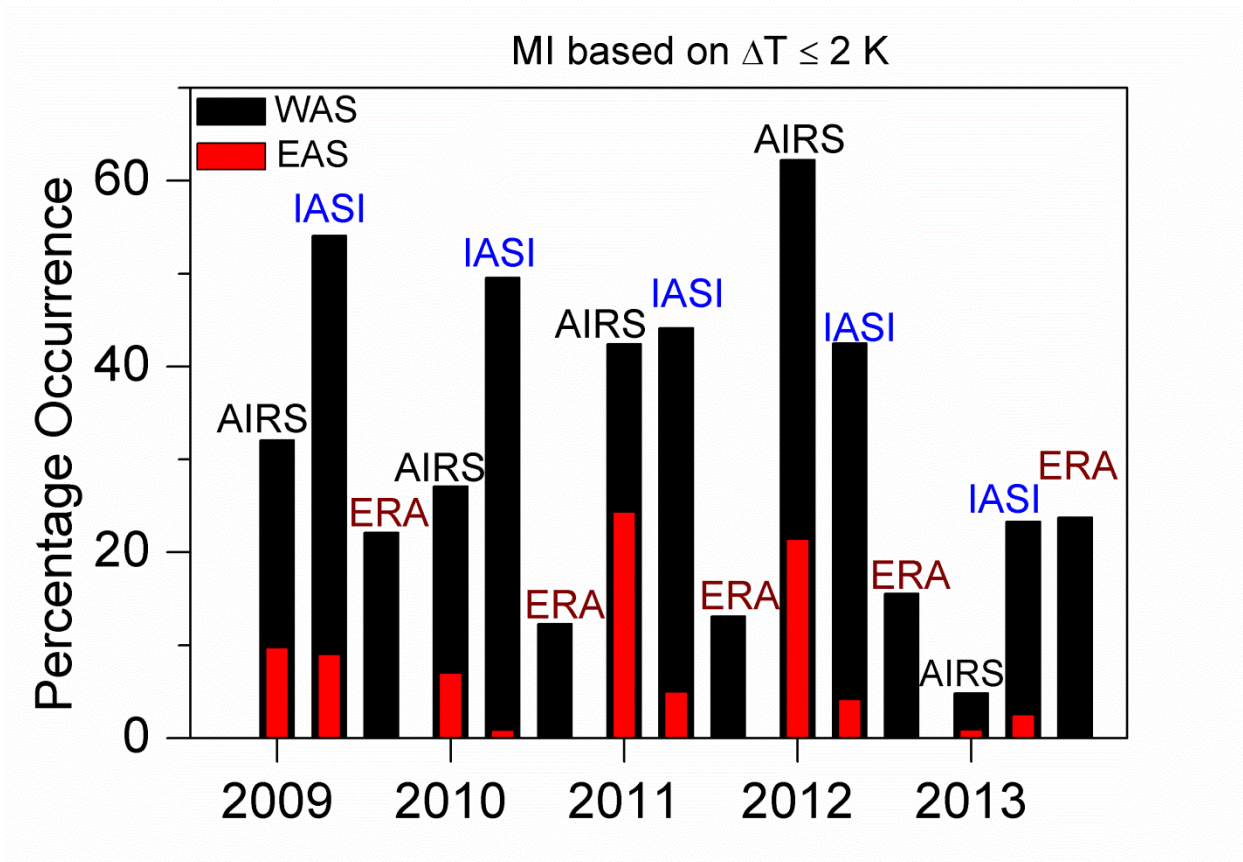
726

727

728

729

730



732

733 **Figure 8.** Percentage occurrence of MI observed with (a) $\Delta T \leq 2K$ using IASI, AIRS and ERA-

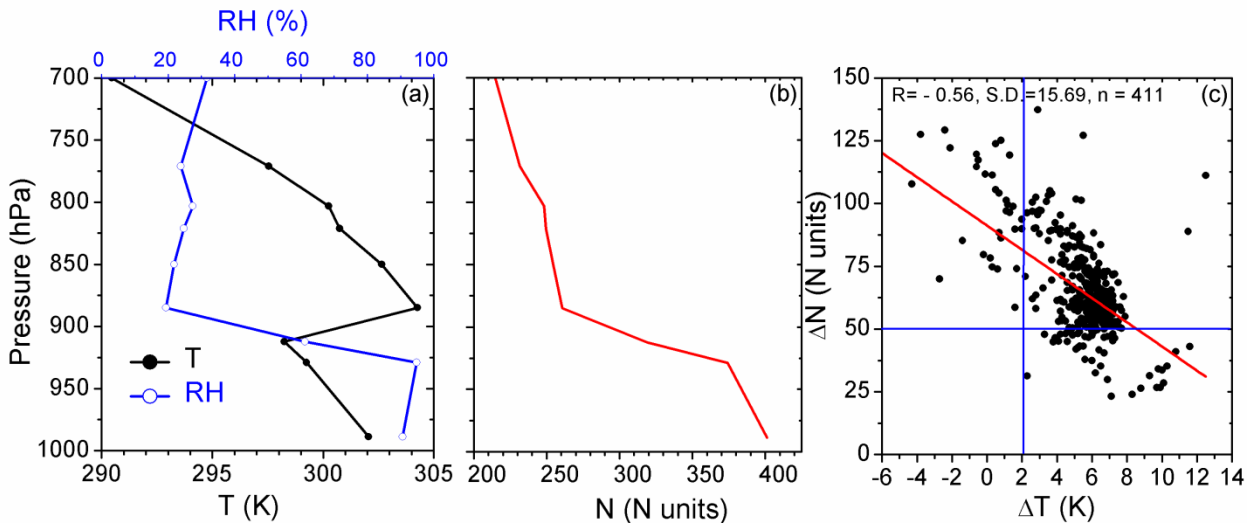
734 Interim data during monsoon seasons of 2009-2013 over WAS and EAS.

735

736

737

738



739

740 **Figure 9.** Typical examples showing MI in temperature and RH on (a) 27 June 1979 at 0656 GMT at
 741 20°N, 62°E obtained from dropsondes from MONEX experiment, (b) N profile (c) Scatter plot of
 742 ΔT and ΔN .

743

744

745

746

747

748

749

750

751

752

753

754

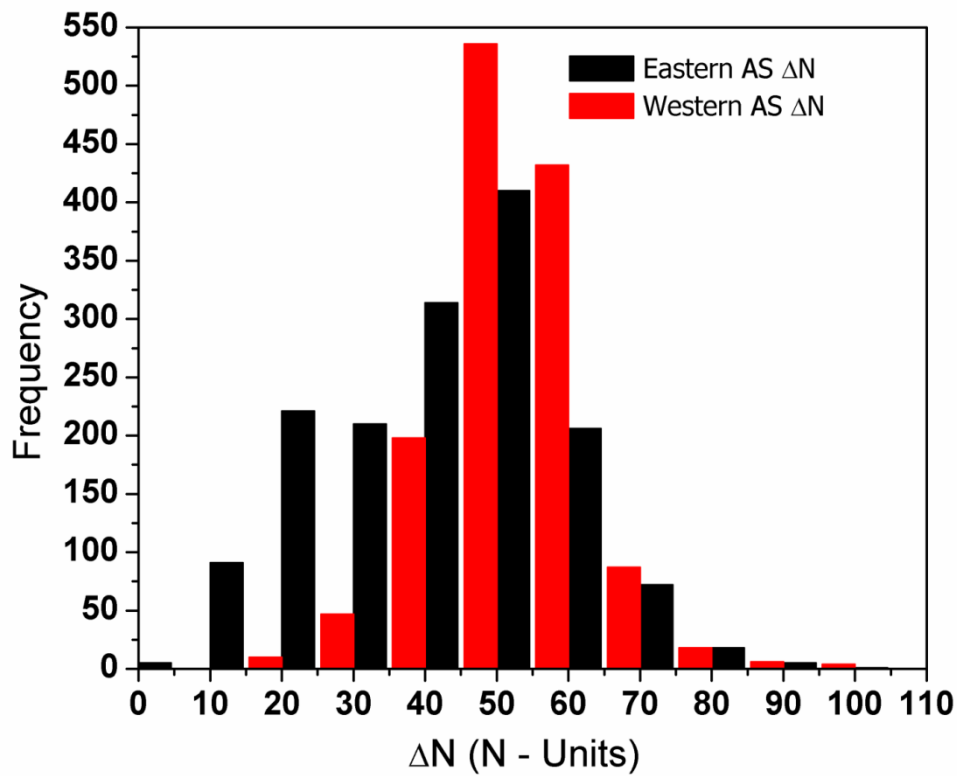
755

756

757

758

759



760

761

762 **Figure 10.** Frequency of ΔN observed in Western AS and Eastern AS during monsoon season of the
763 years 2009-2013 for various ranges of ΔN by COSMIC. Western AS is showing higher values
764 means inversion is there.

765